Search in the Two-Photon Final State for Evidence of New Particle Production at the Large Hadron Collider

Rachel P. Yohay
University of Virginia
rpy3y@virginia.edu

December 31, 2011

Contents

1 Introduction **3**

2 Overview of the Standard Model of Particle Physics **4**
2.1 Particle Content 6
2.2 Electroweak Symmetry Breaking and the Higgs Mechanism 6
2.3 The Hierarchy Problem, The Origins of Mass, and Fine Tuning 6

3 The Supersymmetric Extension to the Standard Model **7**
3.1 Supermultiplet Representation 7
3.2 The Unbroken SUSY Lagrangian 9
3.3 Soft SUSY Breaking 10
3.4 Dark Matter and the WIMP Miracle 10
3.5 Gauge-Mediated SUSY Breaking 10
3.6 Experimental Status of SUSY 10

4 The Large Hadron Collider **15**

5 The Compact Muon Solenoid Experiment **16**
5.1 The Detectors and Their Operating Principles 16
5.1.1 Tracking System 16
5.1.2 Electromagnetic Calorimeter 16
5.1.3 Hadronic Calorimeter 16
5.1.4 Muon System 16
5.1.5 Far Forward Calorimetry 16
5.2 Triggering, Data Acquisition, and Data Transfer 16
5.2.1 Level 1 and High Level Trigger Systems 16
5.2.2 Data Acquisition System 16
5.2.3 Data Processing and Transfer to Computing Centers 16

6 Event Selection **17**
6.1 HLT 17
6.2 Object Reconstruction 17
6.2.1 Photons 17
6.2.2 Electrons 17
6.2.3 Jets and Missing Transverse Energy 17

6.3 Photon Identification Efficiency 17

7 Data Analysis **18**
7.1 Modeling the QCD Background 18
7.1.1 Systematic Errors 18
7.2 Modeling the Electroweak Background 20
7.3 Results 20

8 Interpretation of Results in Terms of GMSB Models **21**
8.1 Simplified Models 21
8.2 Upper Limit Calculation 21
8.3 Cross Section Upper Limits 21
8.4 Exclusion Contours 21

9 Conclusion **22**

Chapter 1

Introduction

Lorum ipsum fuck Republicans.

Chapter 2

Overview of the Standard Model of Particle Physics

In the 1960s, Sheldon Glashow, Steven Weinberg, and Abdus Salam proposed a mathematical framework that unified the electromagnetic and weak forces at an energy scale in the hundreds of GeV/c, as well as a mechanism for breaking the electroweak symmetry at low energies [1]. At the same time, Murray Gell-Mann introduced the concept of quarks to describe hadron spectroscopy, a concept that would later grow into quantum chromodynamics (QCD), the full theory of the strong force [2]. These two key developments motivated the unified representation of particle physics as a set of fields whose dynamics are invariant under the Standard Model gauge group

$$SU(3)_C \otimes SU(2)_L \otimes U(1)_{EM} \tag{2.1}$$

where $SU(3)_C$ describes the quark QCD interactions, $SU(2)_L$ describes the weak interactions among quarks and leptons, and $U(1)_{EM}$ describes the electromagnetic interaction.

The Standard Model, in particular the electroweak theory, has been an extremely successful predictor of particle production and interaction cross-sections and decay rates, as well as of the exact masses of the electroweak force carriers. The case for the validity of the Standard Model was bolstered by the many precision QCD and electroweak measurements carried out at the Large Electron-Positron (LEP) collider, which ran from 1989-2000 at center-of-mass energies between 65 and 104 GeV/c [3]. Figure 2.1 shows some of the highlights of the LEP program.

However, there are still deep theoretical problems with the Standard Model, stemming from the introduction of the Higgs scalar into the theory to break electroweak symmetry [4]. Since the Higgs self-energy diagram is quadratically sensitive to the ultraviolet cutoff scale(footnote: this is a general property of scalar fields), and assuming that there are no new important energy scales of physics between the weak scale ($\mathcal{O}(10^2$ GeV/c)) and the Planck scale ($\mathcal{O}(10^{19}$ GeV/c)), in order to be consistent with experimental measurements, this diagram must include a remarkable 17-orders-of-magnitude cancellation that is otherwise poorly motivated [5]. The quest to find new physics at an intermediate energy scale between the weak and Planck scales, and

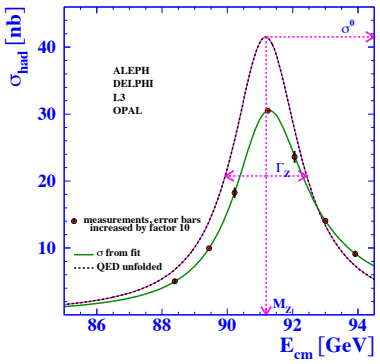

(a) Total hadronic cross-section as a function of collider center-of-mass energy.

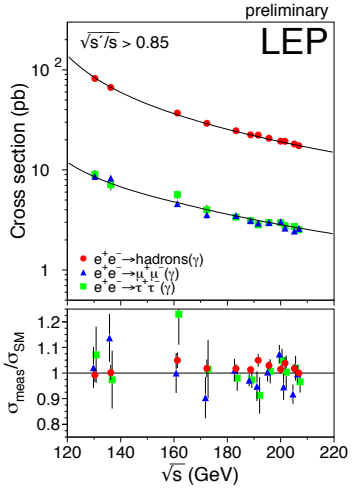

(b) Measured and predicted dependence of the $q\bar{q}$, $\mu^+\mu^-$, and $\tau^+\tau^-$ pair production cross sections on LEP center-of-mass energy.

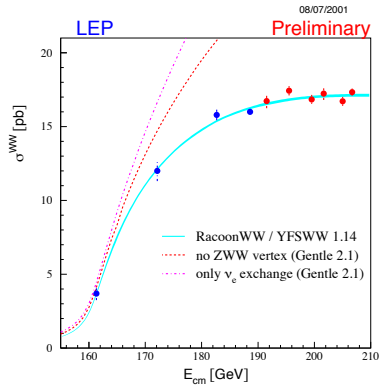

(c) Measured and predicted dependence of the W^+W^- pair production cross section on LEP center-of-mass energy.

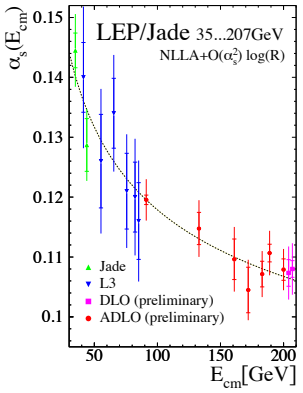

(d) Measured and predicted dependence of the strong coupling constant α_s on LEP center-of-mass energy.

Figure 2.1: Selected LEP measurements demonstrating its contribution to the precise understanding of the Standard Model. Reprinted from [3].

thus extend the Standard Model, was the driving force behind the construction of the Large Hadron Collider (LHC) in 2009, the world's highest energy particle accelerator to date.

In this chapter I will briefly describe the Standard Model particle content, the theory and major results of electroweak symmetry breaking (EWSB), and the problems that the Standard Model is as yet ill-prepared to address.

2.1 Particle Content

2.2 Electroweak Symmetry Breaking and the Higgs Mechanism

2.3 The Hierarchy Problem, The Origins of Mass, and Fine Tuning

Chapter 3

The Supersymmetric Extension to the Standard Model

The following introduction to SUSY focuses primarily on the aspects of the formalism that are relevant to phenomenology. In particular, most of the details of SUSY breaking (about which there is little theoretical consensus) are omitted, except where they are relevant to experiment.

3.1 Supermultiplet Representation

The Standard Model is extended to include supersymmetry by the introduction of a supersymmetry transformation that takes fermionic states to bosonic states and vice versa. In analogy with the known symmetries of the Standard Model, the SUSY transformation has associated generators that obey defining commutation relations, and a fundamental representation. All SM particles and their *superpartners* fall into one of two *supermultiplet* representations. Using the property that

$$n_F = n_B, \tag{3.1}$$

where n_F is the number of fermionic degrees of freedom per supermultiplet and n_B is the number of bosonic degrees of freedom, the two types of supermultiplets are

1. *Chiral supermultiplets*: one Weyl fermion (two helicity states $\Rightarrow n_F = 2$) and one complex scalar field (with two real components $\Rightarrow n_B = 2$)

2. *Gauge supermultiplets*: One spin-1 vector boson (two helicity states $\Rightarrow n_B = 2$) and one Weyl fermion (two helicity states $\Rightarrow n_F = 2$)

In the gauge supermultiplet, the vector boson is assumed massless (i.e. before EWSB generates a mass for it). Since the superpartners to the SM particles have not yet been discovered, they must be significantly heavier than their SM counterparts. Unbroken SUSY predicts that the SM particles and their superpartners must have exactly the same mass, so ultimately a mechanism for SUSY breaking must be introduced to generate masses for the superpartners (see Sec. 3.3). Tables 3.1 and 3.2

show the chiral and gauge supermultiplets of the supersymmetric Standard Model, respectively. Note that the scalar partners to the SM fermions are denoted by placing an "s" in front of their names, while the chiral fermion partners to the SM gauge bosons are denoted by appending "ino" to their names.

Table 3.1: Chiral supermultiplets of the supersymmetric Standard Model. Modified from Table 1.1 of [14].

Type of supermultiplet	Notation	Spin-0 component	Spin-1/2 component	Representation under $SU(3)_C \otimes SU(2)_L \otimes U(1)_Y$
Left-handed quark/squark doublet ($\times$ 3 families)	Q	$(\widetilde{u}_L \ \widetilde{d}_L)$	$(u_L \ d_L)$	$(\mathbf{3}, \mathbf{2}, \frac{1}{6})$
Right-handed up-type quark/squark singlet ($\times$ 3 families)	$\overline{u}$	$\widetilde{u}_R^*$	$u_R^\dagger$	$(\overline{\mathbf{3}}, \mathbf{1}, -\frac{2}{3})$
Right-handed down-type quark/squark singlet ($\times$ 3 families)	$\overline{d}$	$\widetilde{d}_R^*$	$d_R^\dagger$	$(\overline{\mathbf{3}}, \mathbf{1}, \frac{1}{3})$
Left-handed lepton/slepton doublet ($\times$ 3 families)	L	$(\widetilde{\nu}_{eL} \ \widetilde{e}_L)$	$(\overline{\nu}_{eL} \ e_L)$	$(\mathbf{1}, \mathbf{2}, -\frac{1}{2})$
Right-handed lepton/slepton singlet ($\times$ 3 families)	$\overline{e}$	$\widetilde{e}_R^*$	$e_R^\dagger$	$(\overline{\mathbf{1}}, \mathbf{1}, 1)$
Up-type Higgs/Higgsino doublet	H_u	$(H_u^+ \ H_u^0)$	$(\widetilde{H}_u^+ \ \widetilde{H}_u^0)$	$(\mathbf{1}, \mathbf{2}, \frac{1}{2})$
Down-type Higgs/Higgsino doublet	H_d	$(H_d^0 \ H_d^-)$	$(\widetilde{H}_d^0 \ \widetilde{H}_d^-)$	$(\mathbf{1}, \mathbf{2}, -\frac{1}{2})$

Table 3.2: Gauge supermultiplets of the supersymmetric Standard Model. Modified from Table 1.2 of [14].

Type of supermultiplet	Spin-1/2 component	Spin-1 component	Representation under $SU(3)_C \otimes SU(2)_L \otimes U(1)_Y$
Gluon/gluino	$\widetilde{g}$	g	($\mathbf{8}$, $\mathbf{1}$, 0)
W/wino	$\widetilde{W}^{\pm}$ $\widetilde{W}^0$	$W^{\pm}$ W^0	($\mathbf{1}$, $\mathbf{3}$, 0)
B/bino	$\widetilde{B}^0$	B^0	($\mathbf{1}$, $\mathbf{1}$, 0)

3.2 The Unbroken SUSY Lagrangian

The first piece of the full unbroken SUSY Lagrangian density consists of the kinetic and interacting terms related to the chiral supermultiplets. As explained in Sec. 3.1, a chiral supermultiplet consists of a Weyl fermion ψ (the ordinary fermion) and a complex scalar ϕ (the sfermion). For a collection of such chiral supermultiplets, the Lagrangian is

$$\begin{aligned}\mathcal{L}_{chiral} &= -\partial^\mu \phi^{*i} \partial_\mu \phi_i - V_{chiral}(\phi, \phi^*) - i\psi^{\dagger i}\overline{\sigma}^\mu \partial_\mu \psi_i - \frac{1}{2} M^{ij}\psi_i \psi_j \\ &\quad - \frac{1}{2} M^*_{ij}\psi^{\dagger i}\psi^{\dagger j} - \frac{1}{2} y^{ijk}\phi_i \psi_j \psi_k - \frac{1}{2} y^*_{ijk}\phi^{*i}\psi^{\dagger j}\psi^{\dagger k} \end{aligned} \tag{3.2}$$

where i runs over all supermultiplets in Table **??**, $\overline{\sigma}^\mu$ are -1 $\times$ the Pauli matrices (except for $\sigma^0 = \overline{\sigma}^0$), M^{ij} is a mass matrix for the fermions, y^{ijk} are the Yukawa couplings between one scalar and two spinor fields, and $V_{chiral}(\phi, \phi^*$ is the scalar potential

$$\begin{aligned} V_{chiral}(\phi, \phi^*) &= M^*_{ik} M^{kj} \phi^{*i} \phi_j + \frac{1}{2} M^{in} y^*_{jkn} \phi_i \phi^{*j} \phi^{*k} \\ &\quad + \frac{1}{2} M^*_{in} y^{jkn} \phi^{*i} \phi_j \phi_k + \frac{1}{4} y^{ijn} y^*_{kln} \phi_i \phi_j \phi^{*k} \phi^{*l}. \end{aligned} \tag{3.3}$$

The Lagrangian can also be written as the kinetic terms plus derivatives of the *superpotential* W:

$$\begin{aligned}\mathcal{L}_{chiral} &= -\partial^\mu \phi^{*i} \partial_\mu \phi_i - i\psi^{\dagger i}\overline{\sigma}^\mu \partial_\mu \psi_i \\ &\quad - \frac{1}{2}\left(\frac{\delta^2 W}{\delta\phi^i \delta\phi^j}\psi_i \psi_j + \frac{\delta^2 W^*}{\delta\phi_i \delta\phi_j}\psi^{\dagger i}\psi^{\dagger j}\right) - \frac{\delta W}{\delta\phi^i}\frac{\delta W^*}{\delta\phi_i} \end{aligned} \tag{3.4}$$

where

$$W = M^{ij}\phi_i \phi_j + \frac{1}{6} y^{ijk}\phi_i \phi_j \phi_k. \tag{3.5}$$

The second part of the Lagrangian involves the gauge supermultiplets. In terms of the spin-1 ordinary gauge boson A^a_μ and the spin-1/2 Weyl spinor gaugino λ^a of the gauge supermultiplet, where a runs over the number of generators for the SM subgroup (i.e. 1-8 for $SU(3)_C$, 1-3 for $SU(2)_L$, and 1 for $U(1)_Y$), this part of the Lagrangian is

$$\mathcal{L}_{gauge} \;=\; -\frac{1}{4}F^a_{\mu\nu}F^{\mu\nu a} \;-\; i\lambda^{\dagger a}\overline{\sigma}^\mu D_\mu\lambda^a \;+\; \frac{1}{2}D^aD^a \tag{3.6}$$

where

$$F^a_{\mu\nu} \;=\; \partial_\mu A^a_\nu \;-\; \partial_\nu A^a_\mu \;+\; gf^{abc}A^b_\mu A^c_\nu \tag{3.7}$$

(g is the coupling constant and f^{abc} are the structure constants for the particular SM gauge group),

$$D_\mu\lambda^a \;=\; \partial_\mu\lambda^a \;+\; gf^{abc}A^b_\mu\lambda^c, \tag{3.8}$$

and D^a is an auxiliary field that does not propagate (in the literature, it is used as a bookkeeping tool and can be removed via its algebraic equation of motion).

To build a fully supersymmetric and gauge-invariant Lagrangian, the ordinary derivatives in $\mathcal{L}_{chiral}$ (Eq. 3.2) must be replaced by covariant derivatives

3.3 Soft SUSY Breaking

3.4 Dark Matter and the WIMP Miracle

3.5 Gauge-Mediated SUSY Breaking

3.6 Experimental Status of SUSY

Collider searches for evidence of supersymmetry began in earnest in the 1980s [6] and continue to this day. Most recently, the LHC and Tevatron[1] experiments have set the strictest limits on a variety of SUSY breaking scenarios, including GMSB and mSUGRA (discussed below).

Figure 3.1 shows the current limits set by the CMS experiment on the mSUGRA model (with $\tan\beta = 10$) in the m_0-$m_{1/2}$ plane. (Note that although the plot is truncated at $m_0 = 1000$ GeV/c^2, some searches are sensitive out to $m_0 \sim 2000$ GeV/c^2.) Although the LHC has pushed m_0 above $\sim$1 TeV/c^2 for $m_{1/2}$ up to $\sim$400 GeV/c^2, casting some doubt onto the theory's prospects for solving the hierarchy problem,

[1]Located on the Fermilab site in Batavia, Illinois, the Tevatron was a proton-antiproton collider operating at 1.96 TeV center-of-mass energy. The Tevatron ran from 1987 to 2011 [7].

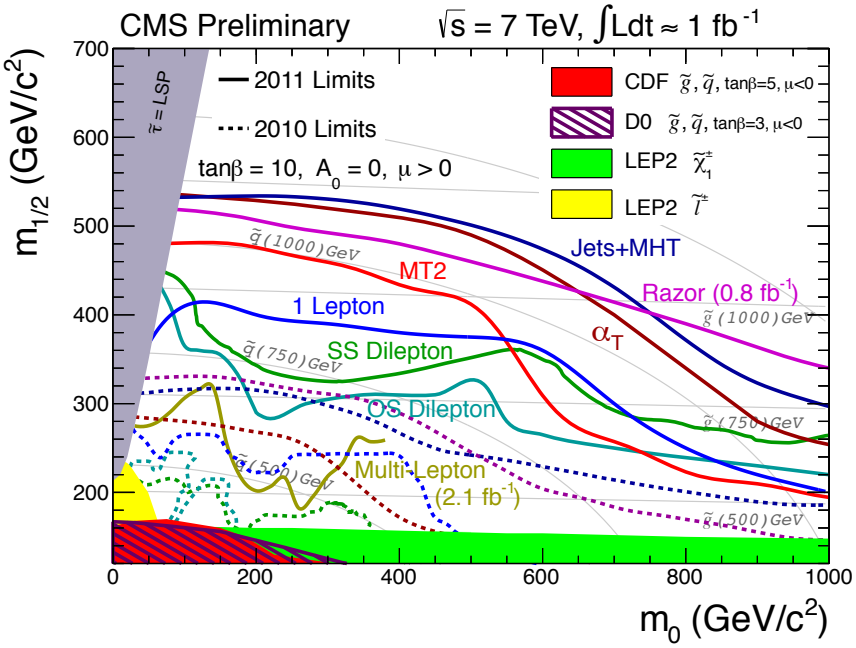

Figure 3.1: CMS limits on mSUGRA with tan $\beta = 10$. The limits set by individual searches are shown as separate colored lines. Solid lines refer to 2011 searches (i.e. using an integrated luminosity of $\sim$1 fb^{-1}), while dashed lines refer to 2010 searches ($\sim$36 pb^{-1}). Reprinted from [9].

there is still a sizable chunk of mSUGRA parameter space that is not ruled out by collider experiments. Furthermore, parts of the CMS unexplored regions overlap with areas allowed by astrophysics experiments [8].

Figure 3.2 shows the most up-to-date limit (using 1 fb^{-1} of integrated luminosity collected by the ATLAS experiment [10] at the LHC) on the Snowmass Points and Slopes (SPS) model of minimal GMSB (mGMSB), dubbed SPS8 [11]. SPS8 represents the simplest class of GMSB models described in Sec. 3.5. The best limits on a variety of general gauge mediation (GGM) models, from the same ATLAS study, are shown in Figure 3.3. In these models, no assumptions are made about the specific parameters common to many gauge mediation models (e.g. the number of messengers or the relationship between the messenger mass and the SUSY breaking scale). Instead, it is only assumed that the lightest neutralino is light enough to be produced on-shell at the LHC (by setting M_1 and M_2 appropriately, see Sec. **??**) and that it decays to a gravitino, that the gravitino is extremely relativistic (mass of order eV-keV), and that the gravitino is stable. The one-dimensional scan over SUSY breaking scales in the SPS8 model (in which the full sparticle spectrum is specified by the model parameters) is replaced by a two-dimensional scan over gluino and lightest neutralino mass in the GGM models (in which all sparticles except the gluino, first- and second-generation squarks, and neutralinos are forced to be at $\sim$1.5 TeV/c^2, effectively decoupling them from the dynamics that can be probed with 1 fb^{-1} at a 7 TeV/c pp collider).

In general, the lifetime of the lightest neutralino in GMSB models can take on any value between hundreds of nanometers to a few kilometers depending on the mass

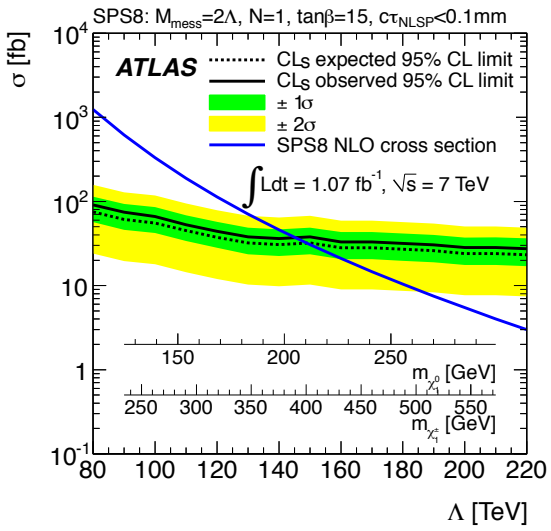

Figure 3.2: ATLAS cross section upper limit on the SPS8 [11] model of mGMSB as a function of SUSY breaking scale Λ, lightest neutralino mass $m_{\tilde{\chi}_1^0}$, or lightest chargino mass $m_{\tilde{\chi}_1^\pm}$. Values of Λ, $m_{\tilde{\chi}_1^0}$, or $m_{\tilde{\chi}_1^\pm}$ below the intersection point between the blue (predicted SPS8 cross section) and black (observed cross section upper limit) curves are excluded. The model parameters listed above the plot are defined in Sec. 3.5. Reprinted from [12].

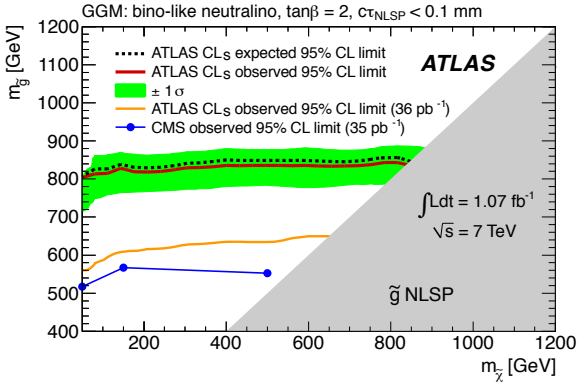

Figure 3.3: ATLAS exclusion contour in the $m_{\tilde{g}}$-$m_{\tilde{\chi}_1^0}$ plane. Values of $m_{\tilde{g}}$-$m_{\tilde{\chi}_1^0}$ below the red curve are excluded. The gray region is theoretically excluded in the GGM models considered. "Bino-like neutralino" means that $M_2 = 1.5$ TeV/c^2. Reprinted from [12].

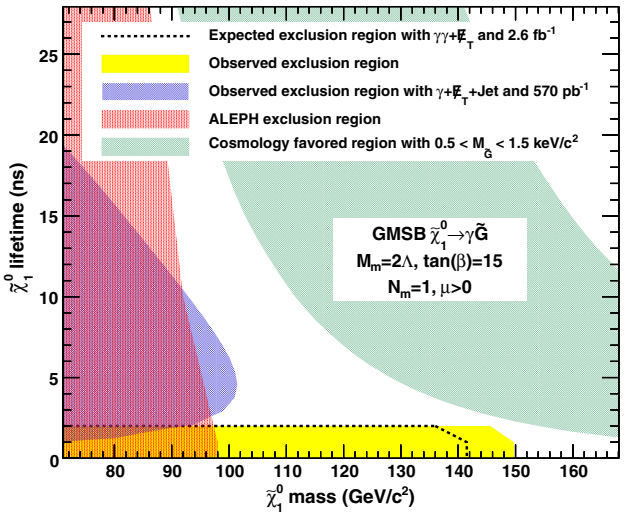

Figure 3.4: CDF exclusion contour in the $\tau_{\widetilde{\chi}_1^0}$-$m_{\widetilde{\chi}_1^0}$ plane, where $\tau_{\widetilde{\chi}_1^0}$ is the lifetime of the neutralino. Reprinted from [13].

of the lightest neutralino and the SUSY breaking scale [14]. The search published in [12] (from which Figs. 3.2 and 3.3 are culled) considers only *prompt* neutralino variants, i.e. with neutralino lifetime short enough that the distance traveled by the neutralino before decay cannot be resolved by the detector. The most recent limits on non-prompt SPS8-style neutralino models were set by the Collider Detector at Fermilab (CDF) collaboration with 570 pb^{-1}, and are shown in Figure 3.4 [13].

Finally, if the gravitino is to make up some or all of the dark matter, constraints on the form of gauge mediation must come from cosmological considerations and astronomical observations. The gravitino in gauge mediation models is usually very light ($\mathcal{O}$(eV-MeV)) because it is proportional to the SUSY breaking scale divided by the Planck mass, and in GMSB the breaking scale is typically only of order a few hundred TeV ([14] and Sec. **??**). A light, highly relativistic dark matter particle might have been produced, for instance, in the early, radiation-dominated period of the universe [15]. This *warm dark matter* (WDM) may be responsible for all of the dark matter needed to account for galactic structure, or it may share the duties with *cold dark matter* (CDM, the classic WIMPs of Sec. **??**). In any viable model, the predicted relic density of the dark matter species must match the observed value of $\Omega h^2 \sim 0.1$ [16]. For many GMSB models, this measurement constrains the gravitino mass to the keV range [17]. This constraint, however, does not translate into a very strong bound on the lifetime of the lightest neutralino. Using the following equation (taken from [17]):

$$\tau_{\widetilde{\chi}_1^0} \sim 130\left(\frac{100\text{GeV}}{m_{\widetilde{\chi}_1^0}}\right)^5\left(\frac{\sqrt{F}}{100\text{TeV}}\right)^4 \mu\text{m} \tag{3.9}$$

where $\sqrt{F}$ is approximately the SUSY breaking scale, and applying the gravitino mass constraint $\sqrt{F} \lesssim 3000$ TeV (cf. Eq. X with $m_{\widetilde{G}} \sim$ keV) and $m_{\widetilde{\chi}_1^0} = 100$ GeV, the upper

bound on the neutralino lifetime is 100 meters. For $\sqrt{F} \sim 100$ TeV, the neutralino lifetime is detectable on collider time scales.

Recently, a lower bound on the WDM particle mass in either pure warm or mixed warm and cold dark matter scenarios was set using observations of the Lyman-α forest. For pure WDM, $m_{WDM} > 8$ keV, while for some mixed WDM-CDM scenarios, $m_{WDM} > 1.1$-1.5 keV [15, 18]. These bounds and others have motivated the development of more complicated gauge mediation models [18]. However, rather than focus on a specific GMSB model, of which there are many, the search detailed here is interpreted in a minimally model dependent way. With this approach, the results can be applied to many competing models. The remainder of this thesis is devoted to the experimental details of the search, analysis strategy, and presentation of the results.

Chapter 4

The Large Hadron Collider

Lorum ipsum fuck Republicans.

Chapter 5

The Compact Muon Solenoid Experiment

5.1 The Detectors and Their Operating Principles

5.1.1 Tracking System

Pixel Detector

Silicon Strip Tracker

5.1.2 Electromagnetic Calorimeter

5.1.3 Hadronic Calorimeter

5.1.4 Muon System

5.1.5 Far Forward Calorimetry

5.2 Triggering, Data Acquisition, and Data Transfer

5.2.1 Level 1 and High Level Trigger Systems

5.2.2 Data Acquisition System

5.2.3 Data Processing and Transfer to Computing Centers

Lorum ipsum fuck Republicans.

Chapter 6

Event Selection

6.1 HLT

6.2 Object Reconstruction

6.2.1 Photons

6.2.2 Electrons

6.2.3 Jets and Missing Transverse Energy

6.3 Photon Identification Efficiency

Lorum ipsum fuck Republicans.

Chapter 7

Data Analysis

7.1 Modeling the QCD Background

7.1.1 Systematic Errors

Jet Energy Scale Uncertainty

The dijet p_T reweighting method utilizes jets corrected for imperfect calorimeter response (see Sec. 6.2.3 for a description of the jet reconstruction and correction procedure). Since the applied jet energy scale (JES) factor has an error associated to it due to the limitations of the JES derivation ([19] and Sec. 6.2.3), this uncertainty must be propagated to the uncertainty on the dijet p_T weights.

The JES contribution to the dijet p_T weights is estimated by performing 1000 pseudo-experiments on each of the $\gamma\gamma$ and ff samples. For the purpose of estimating the JES error, the results of the true experiment may be thought of as a set of measurements:

- The set of **uncorrected jet 4-vectors** corresponding to the **leading EM object** in the $\gamma\gamma$ sample $\left\{p_{j1}^{\mu 1}, p_{j1}^{\mu 2}, ..., p_{j1}^{\mu N_{\gamma\gamma}}\right\}$
- The set of **uncorrected jet 4-vectors** corresponding to the **trailing EM object** in the $\gamma\gamma$ sample $\left\{p_{j2}^{\mu 1}, p_{j2}^{\mu 2}, ..., p_{j2}^{\mu N_{\gamma\gamma}}\right\}$
- The set of **JES** accompanying the uncorrected jet 4-vectors corresponding to the **leading EM object** in the $\gamma\gamma$ sample $\left\{c_{j1}^{1}, c_{j1}^{2}, ..., c_{j1}^{N_{\gamma\gamma}}\right\}$
- The set of **JES** accompanying the uncorrected jet 4-vectors corresponding to the **trailing EM object** in the $\gamma\gamma$ sample $\left\{c_{j2}^{1}, c_{j2}^{2}, ..., c_{j2}^{N_{\gamma\gamma}}\right\}$
- The set of **JES uncertainties** accompanying the uncorrected jet 4-vectors corresponding to the **leading EM object** in the $\gamma\gamma$ sample $\left\{\sigma_{cj1}^{1}, \sigma_{cj1}^{2}, ..., \sigma_{cj1}^{N_{\gamma\gamma}}\right\}$

- The set of **JES uncertainties** accompanying the uncorrected jet 4-vectors corresponding to the **trailing EM object** in the $\gamma\gamma$ sample $\left\{\sigma^1_{cj_2}, \sigma^2_{cj_2}, ..., \sigma^{N_{\gamma\gamma}}_{cj_2}\right\}$
- The set of **uncorrected jet 4-vectors** corresponding to the **leading EM object** in the ff sample $\left\{p^{\mu 1}_{j_1}, p^{\mu 2}_{j_1}, ..., p^{\mu N_{ff}}_{j_1}\right\}$
- The set of **uncorrected jet 4-vectors** corresponding to the **trailing EM object** in the ff sample $\left\{p^{\mu 1}_{j_2}, p^{\mu 2}_{j_2}, ..., p^{\mu N_{ff}}_{j_2}\right\}$
- The set of **JES** accompanying the uncorrected jet 4-vectors corresponding to the **leading EM object** in the ff sample $\left\{c^1_{j_1}, c^2_{j_1}, ..., c^{N_{ff}}_{j_1}\right\}$
- The set of **JES** accompanying the uncorrected jet 4-vectors corresponding to the **trailing EM object** in the ff sample $\left\{c^1_{j_2}, c^2_{j_2}, ..., c^{N_{ff}}_{j_2}\right\}$
- The set of **JES uncertainties** accompanying the uncorrected jet 4-vectors corresponding to the **leading EM object** in the ff sample $\left\{\sigma^1_{cj_1}, \sigma^2_{cj_1}, ..., \sigma^{N_{ff}}_{cj_1}\right\}$
- The set of **JES uncertainties** accompanying the uncorrected jet 4-vectors corresponding to the **trailing EM object** in the ff sample $\left\{\sigma^1_{cj_2}, \sigma^2_{cj_2}, ..., \sigma^{N_{ff}}_{cj_2}\right\}$

From these measurements, the $\gamma\gamma$ and ff dijet p_T spectra and the resulting ff dijet weights can be calculated. In each of the 1000 pseudo-experiments, a new set of JES factors is generated according to the measured JES uncertainties, and new dijet p_T spectra and weights are subsequently calculated. The spread of the 1000 weights (binned in dijet p_T) is taken as the error due to JES uncertainty. The total error on the weights is the quadrature sum of the JES error and the statistical error, and is propagated to the error on the final $\not\!\!E_T$ measurement via a similar pseudo-experiment procedure described in Sec. 7.1.1.[1]

If the JES uncertainty were to cause the jet energy to be reconstructed below the 20 GeV ntuple cut, there could be a small error or bias in the $\not\!\!E_T$ introduced due to EM-matched jets falling below the matching threshold. The percentage of jets lost due to jet E_T matching threshold has been checked in data, and found to be X% (X% of events). Furthermore, the trailing EM E_T cut is 25 GeV/c, implying that the JES would have to be mis-measured by at least 20% to fall below the jet matching threshold. Since the typical JES uncertainty is no more than 5%, a mis-measurement of this type is a 4σ event and should occur in only 0.1% of cases. As expected, this effect is negligible, as shown in Figure X.

[1]The $\not\!\!E_T$ is uncorrected and therefore its central value per event is unaffected by a change in the JES.

Statistical Uncertainty in the ff or ee Weights

7.2 Modeling the Electroweak Background

7.3 Results

Lorum ipsum fuck Republicans.

Chapter 8

Interpretation of Results in Terms of GMSB Models

8.1 Simplified Models

8.2 Upper Limit Calculation

8.3 Cross Section Upper Limits

8.4 Exclusion Contours

Lorum ipsum fuck Republicans.

Chapter 9

Conclusion

Lorum ipsum fuck Republicans.

Bibliography

[1] S.L. Glashow, J. Iliopoulis, and L. Maiani, *Phys. Rev. D* **2** (1970) 1285; S.L. Glashow, *Nucl. Phys.* **22(4)** (1961) 579; J. Goldstone, A. Salam, and S. Weinberg, *Phys. Rev.* **127** (1962) 965; S. Weinberg, *Phys. Rev. Lett.* **19** (1967) 1264; A. Salam and J.C. Ward, *Phys. Lett.* **13(2)** (1964) 168.

[2] M. Gell-Mann, *Phys. Lett.* **8** (1964) 214; G. Zweig, *CERN* **8419/TH. 412** (1964) (unpublished).

[3] J. Drees, *Int. J. Mod. Phys.* **A17** (2002) 3259.

[4] P.W. Higgs, *Phys. Lett.* **12(2)** (1964) 132; P.W. Higgs, *Phys. Rev. Lett.* **13** (1964) 508; P.W. Higgs, *Phys. Rev.* **145** (1966) 1156.

[5] I. Aitchison, *Supersymmetry in Particle Physics: An Elementary Introduction* (Cambridge University Press, Cambridge 2007), p. 4.

[6] E. Fernandez et al., *Phys. Rev. Lett.* **54** (1985) 1118; E. Fernandex et al., *Phys. Rev.* **D35** (1987) 374; D. Decamp et al., *Phys. Lett.* **B237(2)** (1990) 291; F. Abe et al., *Phys. Rev. Lett.* **75** (1995) 613; S. Abachi et al., *Phys. Rev. Lett.* **75** (1995) 618; G. Alexander et al., *Phys. Lett.* **B377(4)** (1996) 273; S. Aid et al., *Z. Phys.* **C71(2)** (1996) 211; S. Aid et al., *Phys. Lett.* **B380(3-4** (1996) 461; B. Aubert et al., *Phys. Rev. Lett.* **95** (2005) 041802.

[7] `http://en.wikipedia.org/wiki/Tevatron`.

[8] O. Buchmueller et al., *CERN-PH-TH/2011-220* (2011).

[9] `https://twiki.cern.ch/twiki/bin/view/CMSPublic/PhysicsResultsSUS`.

[10] G. Aad et al., *JINST* **3** (2008) S08003.

[11] B.C. Allanach et al., *Eur. Phys. J.* **C25** (2002) 113.

[12] G. Aad et al., *CERN-PH-EP-2011-160* (2011).

[13] T. Aaltonen et al., *Phys. Rev. Lett.* **104** (2010) 011801.

[14] S. P. Martin, *A Supersymmetry Primer* **v4** (2006) 86. arXiv:hep-ph/9709356.

[15] A. Boyarsky, J. Lesgourgues, O. Ruchayskiy, and M. Viel, *CERN-PH-TH/2008-234* (2009).

[16] E. Komatsu et al., *Astrophys. J. Suppl. Ser.* **180** (2009) 330.

[17] C.-H. Chen and J.F. Gunion, *Physical Review* **D58** (1998) 075005.

[18] F. Staub, W. Porod, J. Niemeyer, *JHEP* **1001** (2010) 058.

[19] S. Chatrchyan et al., *JINST* **6** (2011) P11002.